Available online at www.sciencedirect.com
ScienceDirect
Applied Catalysis B: Environmental 83 (2008) 277–285
APPLIED CATALYSIS B: ENVIRONMENTAL
www.elsevier.com/locate/apcatb

The effect of Pt on the photocatalytic degradation pathway of methylene blue over TiO_2 under ambient conditions

Zhiqiang Yu, Steven S.C. Chuang *

Department of Chemical and Biomolecular Engineering, University of Akron, 200 E.Buchtel Commons, Akron, OH 44325-3906, USA

Received 6 November 2007; received in revised form 20 January 2008; accepted 26 January 2008
Available online 26 February 2008

Abstract

Photocatalytic degradation pathway of methylene blue (MB) has been studied over TiO_2, 0.5 wt.% Pt/TiO_2, and 3 wt.% Pt/TiO_2 at ambient conditions (30 °C and 1 atm of air) by infrared (IR) spectroscopy. The reaction was proposed to be initiated via the abstraction of H from MB molecule by hydroxyl radical (·OH), followed by $–CH_3$ elimination and $C_{Ar}–N$ scission. The correlation in IR intensity between the decrease in C–H bond in MB molecule and the increase in hydroxyl group (–OH) at 3672 cm^{-1} during the reaction (i) provides an indirect evidence to support the proposed ·OH-initiating pathway, (ii) suggests that the –OH sites could be related to $^{\bullet}OH$ generation sites, and (iii) offers new insights into the photoinduced hydrophilicity of the TiO_2 surface. Subsequent breakup of the MB central ring via accepting protons and photogenerated electrons resulted in the formation of intermediates containing C=O, COO^-, and N–H groups.

Deposition of 0.5 wt.% Pt to TiO_2 enhanced (i) the scission of and C–H bonds and (ii) the formation of intermediates containing C=O and COO^- groups. The latter suggests that Pt provided the sites for oxygen absorption, accelerating the formation rate of oxygen-containing intermediates. The comparable IR intensity of –OH at 3632 cm^{-1} before reaction and –OH at 3672 cm^{-1} during the reaction on TiO_2 and 0.5 wt.% Pt/TiO_2 indicates that $^{\bullet}OH$ generation sites were not blocked by low Pt loading (i.e., 0.5 wt.%). The simultaneous presence of $^{\bullet}OH$ generation, photoelectron generation, and Pt sites could play a synergetic role in enhancing and C–H bond scission and formation of C=O and COO^- species. Increasing Pt loading to 3 wt.% resulted in the total elimination of –OH and the significant decrease in the MB degradation rate, indicating that the low activity of 3 wt.% Pt/TiO_2 could be attributed to the blocking of $^{\bullet}OH$ generation sites by the high Pt loading.

Keywords: Photocatalytic degradation; Titanium dioxide; Hydroxyl group; Photogenerated electron; Infrared spectroscopy

1. Introduction

Titanium dioxide (TiO_2), a semiconductor with a bandgap of 3.0–3.2 eV, has been widely studied for photocatalytic degradation of organics due to its high activity, high stability, and toxicity-free nature [1–6]. Exposure of TiO_2 to UV illumination excites the valence electrons (e^-) to the conduction band, resulting in generation of holes (h^+), as shown in the following step:

$$TiO_2 + h\nu \rightarrow h^+ + e^- \quad (1)$$

The photogenerated electrons may recombine with holes or react with adsorbed oxygen (O_{ad}) on the TiO_2 surface to produce oxygen ions (O_2^-), step (2). O_2^- can further react with adsorbed H_2O (H_2O_{ad}) to produce hydroxyl group (–OH) and hydroxyl radical ($^{\bullet}OH$), step (3)

$$O_{2ad} + e^- \rightarrow O_2^- \quad (2)$$

$$2O_2^- + 2H_2O_{ad} \rightarrow 2OH^{\bullet} + 2OH^- + O_2 \quad (3)$$

In addition to recombination with electrons, the photogenerated holes may react directly with organic compounds in step (4), with H_2O_{ad} to form $^{\bullet}OH$ in step (5), and with H_2O_{ad} at a surface lattice O site in step (6) [7,8].

$$RH + h^+ \rightarrow R^{\bullet} + H^+ \quad (4)$$

$$H_2O_{ad} + h^+ \rightarrow OH^{\bullet} + H^+ \quad (5)$$

$$[Ti{-}O{-}Ti]_s + h^+ + H_2O_{ad} \rightarrow [Ti{-}O^{\bullet}HO{-}Ti]_s + H^+ \quad (6)$$

The $^{\bullet}OH$ and O_2^- have been shown to be present during the photocatalytic degradation of many organics, providing

* Corresponding author. Tel.: +1 330 972 6993; fax: +1 330 972 5856.
E-mail address: schuang@uakron.edu (S.S.C. Chuang).

0926-3373/$ – see front matter
doi:10.1016/j.apcatb.2008.01.040

indirect evidence to support the above reaction steps [3,9–17]. Recent studies have further shown that UV illumination of TiO_2 in the absence of H_2O_{ad} results in h^+-initiating photocatalytic degradation, step (4), and the accumulation of photogenerated electrons in the conduction band of TiO_2 [15]. The presence of a limited quantity of H_2O_{ad} on TiO_2 facilitates the reactions dealing with $^{\bullet}OH$, step (5), leading to $^{\bullet}OH$-initiating photocatalytic degradation [14,15]. An understanding of the role of H_2O_{ad} could assist in designing the photocatalytic degradation process since majority of these practical processes involve H_2O-containing streams.

To develop a practical TiO_2-based photocatalytic process, majority of studies on TiO_2 focused on either enhancing its photocatalytic activity or extending its absorption spectrum from UV to the visible range by adding a second element to the TiO_2 bulk structure [18–20]. Pt/TiO_2 has been reported to exhibit enhanced photocatalytic activity compared to TiO_2. Pt enhancement has been attributed to (i) increasing formation of $^{\bullet}OH$ and oxygen species by trapping photogenerated electrons on Pt [19,21] and (ii) providing thermal catalytic sites for adsorbed species and reaction intermediates [22–25]. Interestingly, Pt has also been observed to inhibit photocatalytic degradation on TiO_2. The Pt inhibition could be resulted from the blocking of TiO_2 active sites by excess Pt deposition [26,27], the presence of inactive Pt oxide [19,21,28,29], and Pt-promoted recombination of electrons and holes [27,30,31]. Resolving the effect of Pt deposition on TiO_2 is essential for developing a better understanding of pathways and effective catalysts for photocatalytic degradation reactions.

The objective of this study is to investigate the Pt effect on the methylene blue (MB) photocatalytic degradation on TiO_2. MB, a typical textile dye, is used as model compound here because it has provided a simple and standard way to measure the photocatalyst activity in liquid phase reactions [14,32–34]. MB molecule contains several types of bonds, such as C–H, N–CH_3, C=N, C=S, C_{Ar}–N, and aromatic rings, as shown in Fig. 1(a), and thus serves as an excellent model compound for investigating the specific effect of Pt on scission rates of various MB bonds by infrared (IR) spectroscopy. IR technique is especially sensitive for determining the relative rate of scission and formation of the bonds which are IR-active (i.e., polar bonding). Determining the Pt effect on scission rates of specific MB bonds as well as the formation rates of intermediate species and H_2O_{ad} shed the light into the role of Pt in the reaction pathway of the photocatalytic degradation of organics over TiO_2 catalysts.

2. Experimental

2.1. Materials

Titanium dioxide (TiO_2) was supplied by Degussa (P-25, surface area ~50 m^2/g; mean diameter ca. 30 nm; 80% anatase, and 20% rutile). MB ($C_{16}H_{18}ClN_3S^{\bullet}3H_2O$), chloroplatinic acid hexahydrate(IV), and CaF_2 powder (325 mesh) were purchased from Alfa Aesar. All compounds were used without further treatments.

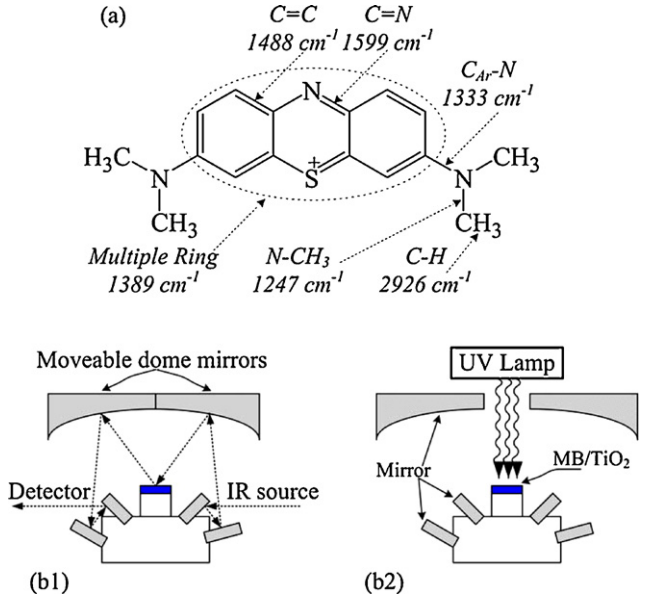

Fig. 1. (a) MB molecular structure and experimental apparatus for (b1) collecting IR spectra and (b2) carrying out the MB photocatalytic degradation.

2.2. Catalyst preparation

0.5 wt.% Pt/TiO_2, 1 wt.% Pt/TiO_2, and 3 wt.% Pt/TiO_2 were prepared separately by the photodeposition method [28,35,36]. In preparation of 0.5 wt.% Pt/TiO_2, 100 mg TiO_2 were suspended in 30 mL aqueous solution with 1.4 mg chloroplatinic acid hexahydrate in a rectangular quartz reactor. The suspending solution was ultrasonicated for 20 min and then deoxygenized by N_2-bubbling for 30 min before UV illumination. A 350 W mercury UV lamp (Oriel 6286) with an intensity of 40 mW/cm^2 and a full UV–visible light range was used for initiating Pt deposition onto TiO_2 in the suspending solution with magnetic stirring for 24 h. The color of the suspending solution changed from white to gray after 2 h of UV illumination. The resulting catalyst was centrifuged and washed with deionized water five times to remove the undesirable ions and then dried under vacuum oven at 100 °C. 3 wt.% Pt/TiO_2 was prepared by the same approach using 100 mg TiO_2 and 4.2 mg of chloroplatinic acid hexahydrate.

2.3. Catalysts characterization

The crystalline structure of the catalysts was characterized by powder X-ray diffraction (XRD) using a Philips APD3700 X-ray Diffractometer equipped with a Cu Kα (wavelength: 1.5406 Å). XRD pattern was recorded from 2° to 60° (2θ) with a step size of 0.02° and a time step of 1.0 s. UV–visible diffuse reflectance spectra of catalysts were recorded by a HITACHI (U-3010) spectrophotometer with a HARRICK (HVC-DRP) diffuse reflectance accessory. The particle size of catalysts was analyzed by the transmission electron microscope (TEM, FEI-TACNAI 12).

2.4. Experimental apparatus

Adsorption of 5 wt.% MB on the various catalysts was achieved by mixing 19 mg of catalyst and 1 mL of MB aqueous solution with a concentration of 1 mg/mL and then vacuum-drying at 80 °C for 24 h. 5 wt.% MB on CaF_2 powder was prepared by the same way for the blank experiment.

5 wt.% adsorbed MB on catalysts was ground and placed in a diffuse reflectance infrared Fourier transform spectroscopy (DRIFTS) cell, as shown in Fig. 1. The moveable dome mirrors of the DRIFTS cell were closed for collecting IR spectra and open for carrying out the MB photocatalytic degradation. Since the DRIFTS cell was not sealed, the gaseous CO_2 produced from the reaction were removed from the catalyst by the dry purging air connected to the IR bench (Nicolet Magna 560). MB degradation over TiO_2, 0.5 wt.% Pt/TiO_2, 3 wt.% Pt/TiO_2, and CaF_2 was carried out using a Xe 350 W mercury lamp (Oriel 6286) with an intensity of 16.7 mW/cm^2 and a full UV–visible light range at 30 °C. Shutting off UV illumination allowed the catalyst to cool down to room temperature.

IR spectra were collected by co-added 32 scans at a resolution of 4 cm^{-1} and presented in two formats: (i) single-beam spectrum and (ii) difference spectrum. Single-beam spectrum is a plot of raw detector response, where absorbance of IR-active species is shown in a negative direction [37]. The difference spectrum during the MB degradation was obtained by subtracting the single-beam spectrum of MB/catalyst before the reaction from the single-beam spectrum of MB/catalyst during the reaction. The positive peak is resulted from the species formed during the reaction; the negative peak indicates the consumption of the adsorbed species. The formula for calculating IR intensity (A) of a species in the difference spectrum is as follows: $A(v) = -\log\{I_t(v)/I_{t=0}(v)\}$, where $I_t(v)$ and $I_{t=0}(v)$ refer to IR detector responses of MB/catalyst at the reaction time of t and before the reaction ($t = 0$ min), respectively; v is the wavenumber in the unit of cm^{-1}.

3. Results

Fig. 2 shows the XRD patterns of TiO_2, 0.5 wt.% Pt/TiO_2, 1 wt.% Pt/TiO_2, and 3 wt.% Pt/TiO_2. The Pt peak (1 1 1) at 39.8° was absent in the XRD pattern of 0.5 wt.% Pt/TiO_2 because of low Pt loading. TEM image of 0.5 wt.% Pt/TiO_2 in Fig. 3(a) shows the presence of Pt particles. The appearance of the Pt(1 1 1) peak in the XRD pattern of 3 wt.% Pt/TiO_2 indicates that the bulk of the Pt particle was in the reduced state. The crystallite sizes of TiO_2 and Pt particles were determined to be 11.0 and 3.5 nm respectively on 3 wt.% Pt/TiO_2 by the Scherrer equation. The Pt particle size calculated from XRD pattern was consistent with the particle size observed in TEM images, where the large particles correspond to TiO_2 catalyst, and the small and dark spots represent Pt particles.

Fig. 4 presents the UV–visible diffuse reflectance spectra of TiO_2, 0.5 wt.% Pt/TiO_2, 1 wt.% Pt/TiO_2, and 3 wt.% Pt/TiO_2. The absorption of these catalysts in the range of 420–800 nm increased with Pt loading due to the decrease in reflectivity. The diminished reflectivity of Pt/TiO_2 was evidenced by appearance of the black color (i.e., high absorption of visible light) of Pt/TiO_2 particles. The same onset of UV absorption of these catalysts implies that they exhibited the same band gap under UV illumination.

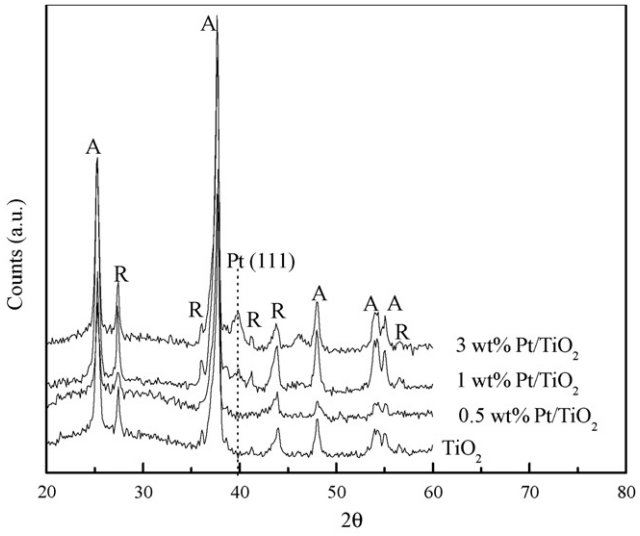

Fig. 2. XRD patterns of TiO_2, 0.5 wt.% Pt/TiO_2, 1 wt.% Pt/TiO_2, and 3 wt.% Pt/TiO_2. A stands for anatase; R stands for rutile.

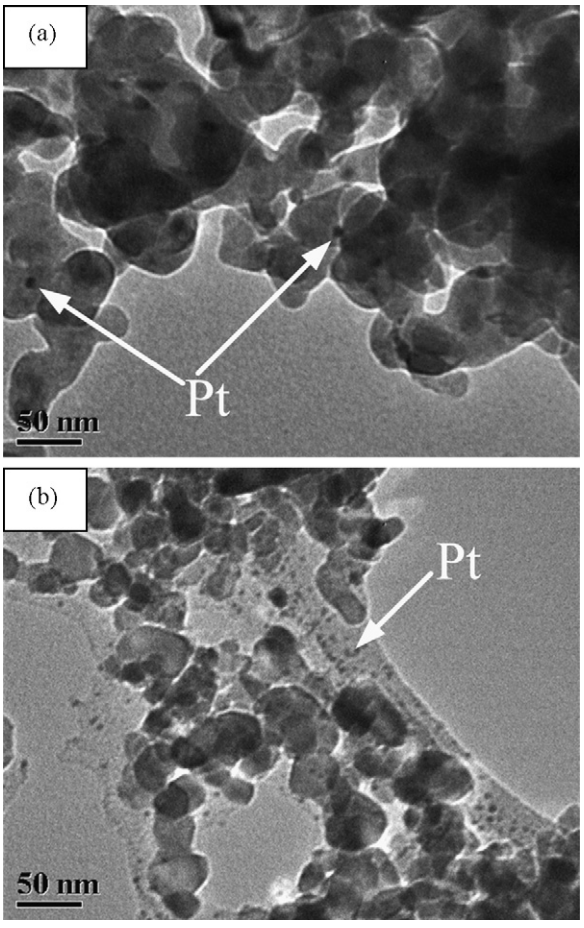

Fig. 3. TEM images of (a) 0.5 wt.% Pt/TiO_2 and (b) 3 wt.% Pt/TiO_2.

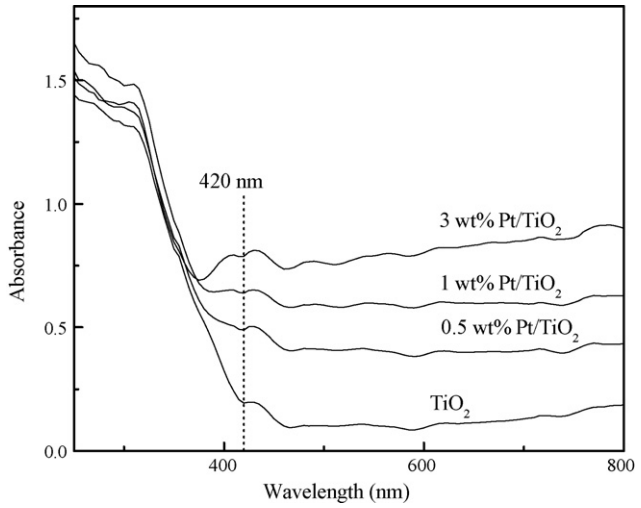

Fig. 4. UV–visible diffuse reflectance spectra of TiO_2, 0.5 wt.% Pt/TiO_2, 1 wt.% Pt/TiO_2, and 3 wt.% Pt/TiO_2.

Fig. 5 compares the initial single-beam spectra of CaF_2, TiO_2, and 0.5 wt.% Pt/TiO_2, and 3 wt.% Pt/TiO_2, as well as adsorbed MB on CaF_2 and these catalysts. CaF_2, which has an excellent infrared transparency above 1000 cm^{-1}, was used to disperse MB. MB molecule on CaF_2 exhibited characteristic bands: C=N central ring stretching at 1599 cm^{-1}, C=C in side aromatic ring stretching at 1488 cm^{-1}, the multiple ring stretching at 1389 cm^{-1}, and the C_{Ar}–N (i.e., the bond between the side aromatic ring and the nitrogen atom) stretching at 1333 cm^{-1}. The band assignments are listed in Table 1. Adsorbed MB on the catalyst surface appeared to remove –OH

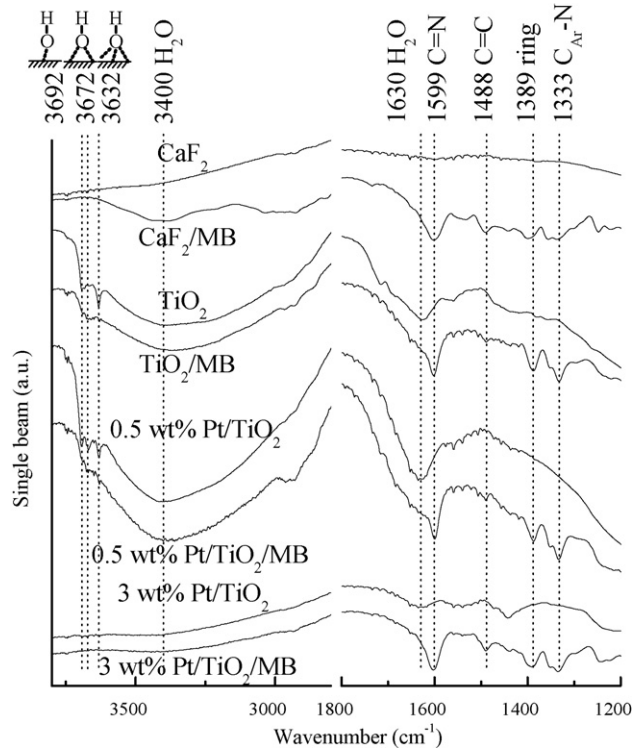

Fig. 5. IR single-beam spectra of CaF_2, TiO_2, 0.5 wt.% Pt/TiO_2, and 3 wt.% Pt/TiO_2, as well as adsorbed MB on CaF_2 and catalysts.

Table 1
Band assignments and their vibration modes

Species	Bands (cm^{-1}) and modes	Reference
MB	$\nu_{as}(CH_3)$/2926; ν(C=N)/1599; ν(C=C)/1488; ν(multiple ring) /1389; $\nu(C_{Ar}–N)$/1333; $\nu(N–CH_3)$ /1247, 1176, 1145	[14,45,62]
RNH_3^+	ν(N–H)/3163; δ_{as}(N–H)/1650	[44,63]
RC=O	ν(C=O)/1714	[14,45]
$RCOO_{ad}^-$	ν(COO)/1575	[45,64,65]
–OH	ν(OH) linear/3692; ν(OH) bridged /3672; ν(OH) triple coordinated/3632;	[43–45]
H_2O_{ad}	ν(HO···H)/3550, 3400; δ(HO···H)/1630	[14,15]
SO_4^{2-}	ν(S–O)/1231	[45]
CO_2	ν_{as}(C=O)/2362	[15]

at 3632 cm^{-1}, indicating adsorbed MB covered part of –OH sites on TiO_2 and 0.5 wt.% Pt/TiO_2. 3 wt.% Pt/TiO_2 did not possess –OH as evidenced by the IR spectrum, suggesting the high Pt loading completely blocked the –OH sites.

Figs. 6–8 show the IR difference spectra taken during the MB degradation from 0 to 240 min on the catalysts. The IR difference spectra were obtained by subtracting the single-beam spectrum at 0 min (i.e., prior to the reaction) from the subsequent single-beam spectra, highlighting the subtle variations of IR bands during the MB degradation. The negative bands manifest the scission of the specific MB bonds

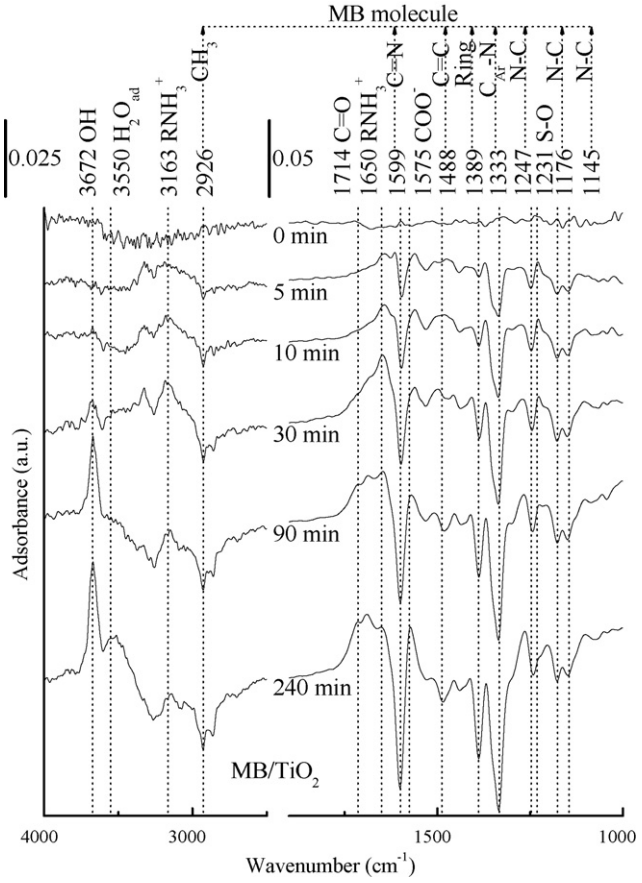

Fig. 6. IR difference spectra during 240 min of the MB photocatalytic degradation on TiO_2.

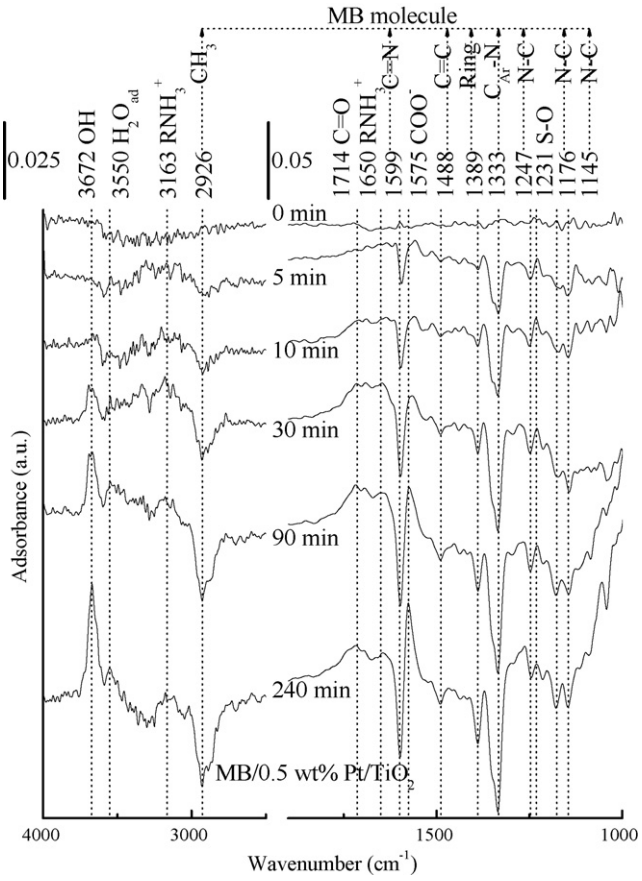

Fig. 7. IR difference spectra during 240 min of the MB photocatalytic degradation on 0.5 wt.% Pt/TiO_2.

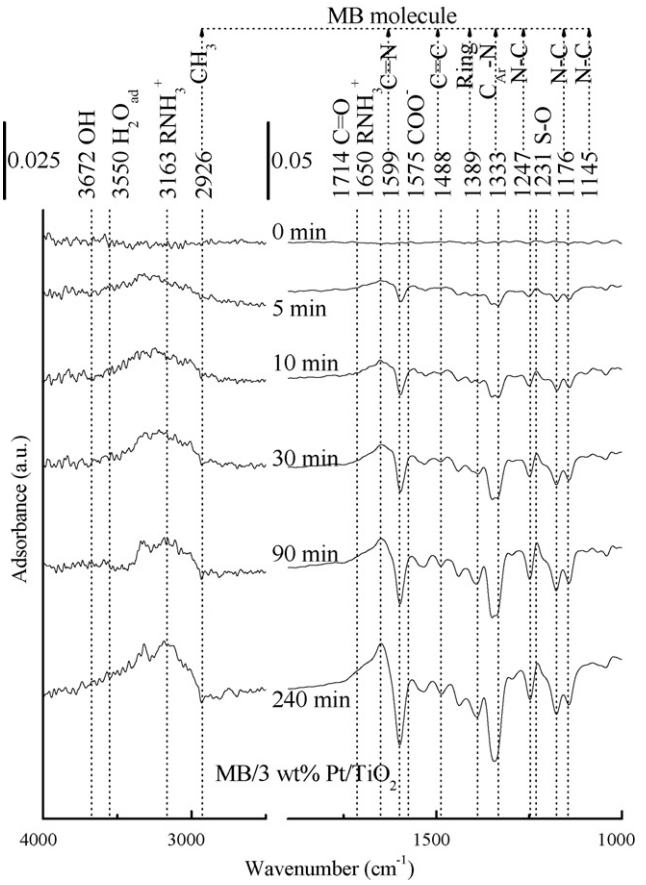

Fig. 8. IR difference spectra during 240 min of the MB photocatalytic degradation on 3 wt.% Pt/TiO_2.

whereas the positive bands reflect the formation of reaction intermediates and products. As the MB photocatalytic degradation proceeded on catalysts, the intensities of MB characteristic bands decreased with reaction time as evidenced by increases in their negative intensities. Previous studies have shown that the scission rates of MB bands on TiO_2 decrease in the order: N–CH_3 at 1247 cm^{-1} > C_{Ar}–N at 1333 cm^{-1} > C═N at 1599 cm^{-1} > the multiple ring stretching at 1389 cm^{-1} > at C═C 1488 cm^{-1} during the first 10 min of the reaction in a sealed DRIFTS reactor [14]. Plotting the intensities of MB bands with time in Fig. 9 shows the scission rates of MB bonding (i.e., the slope of the declining curves) on TiO_2 in this study followed the same decreasing order.

The decrease in MB characteristic bands was accompanied by the emergence of the isolated –OH at 3672 cm^{-1}, H_2O_{ad} at 3550 cm^{-1}, RNH_3^+ at 3163 cm^{-1}, C═O (i.e., the carbonyl bond of an aldehyde) at 1714 cm^{-1}, RNH_3^+ at 1650 cm^{-1}, SO_4^{2-} at 1231 cm^{-1}, and carboxylate (COO^-) at 1575 cm^{-1}. The detailed IR band assignments of these emerging bands are summarized in Table 1.

Figs. 6 and 7 show that the most obvious effect of 0.5 wt.% Pt loading was to decrease the bond scission rate of C═N at 1599 cm^{-1} in MB molecule. The variation of IR intensity of MB bands with reaction time in Fig. 9 further revealed that 0.5 wt.% Pt loading increased the scission rates of C–H in methyl group (–CH_3) at 2926 cm^{-1} and C═C bond in the side aromatic ring, but decreased those of C═N in the central ring, multiple ring structure, and C_{Ar}–N during the first 20 min of the reaction. In contrast, 3 wt.% Pt loading slowed down the scission rates of all the MB bonds.

Fig. 10 compares the formation rate of the bonds for reaction intermediate and products during the MB photocatalytic degradation. 0.5 wt.% Pt/TiO_2 gave a higher initial rates of C═O and –OH formation and a higher overall rate of COO^- formation than TiO_2 and 3 wt.% Pt/TiO_2 whereas 3 wt.% Pt/TiO_2 showed a dramatically low rate of –OH and COO^- formation. The delayed C═O formation after 50 min of the reaction on 3 wt.% Pt/TiO_2 may be related to the initial slow C–H scission rate as shown in Fig. 9.

Fig. 11 shows the IR spectra of CO adsorption over (a) 0.5 wt.% Pt/TiO_2 and (b) 3 wt.% Pt/TiO_2 during CO pulse chemisorptions. The CO bands at 2121 cm^{-1}, 2094 cm^{-1}, and 2088/2078 cm^{-1} were assigned to CO–Pt^{2+}, CO–$Pt^{\delta+}$, and CO–Pt^0, respectively [38–40]. These results indicate that the Pt catalyst prepared by the photodeposition method was a mixture of reduced and oxidized Pt. Results of X-ray photoelectron spectroscopy have reported the presence of oxidized Pt in the Pt/TiO_2 prepared by the photodeposition method [19,31,41]. The IR intensity of CO adsorbed on Pt could reflect the number of Pt site on the catalyst surface. 0.5 wt.% Pt/TiO_2 exhibited higher ratio of the number of oxidized Pt sites to the number of reduced Pt sites than 3 wt.% Pt/TiO_2.

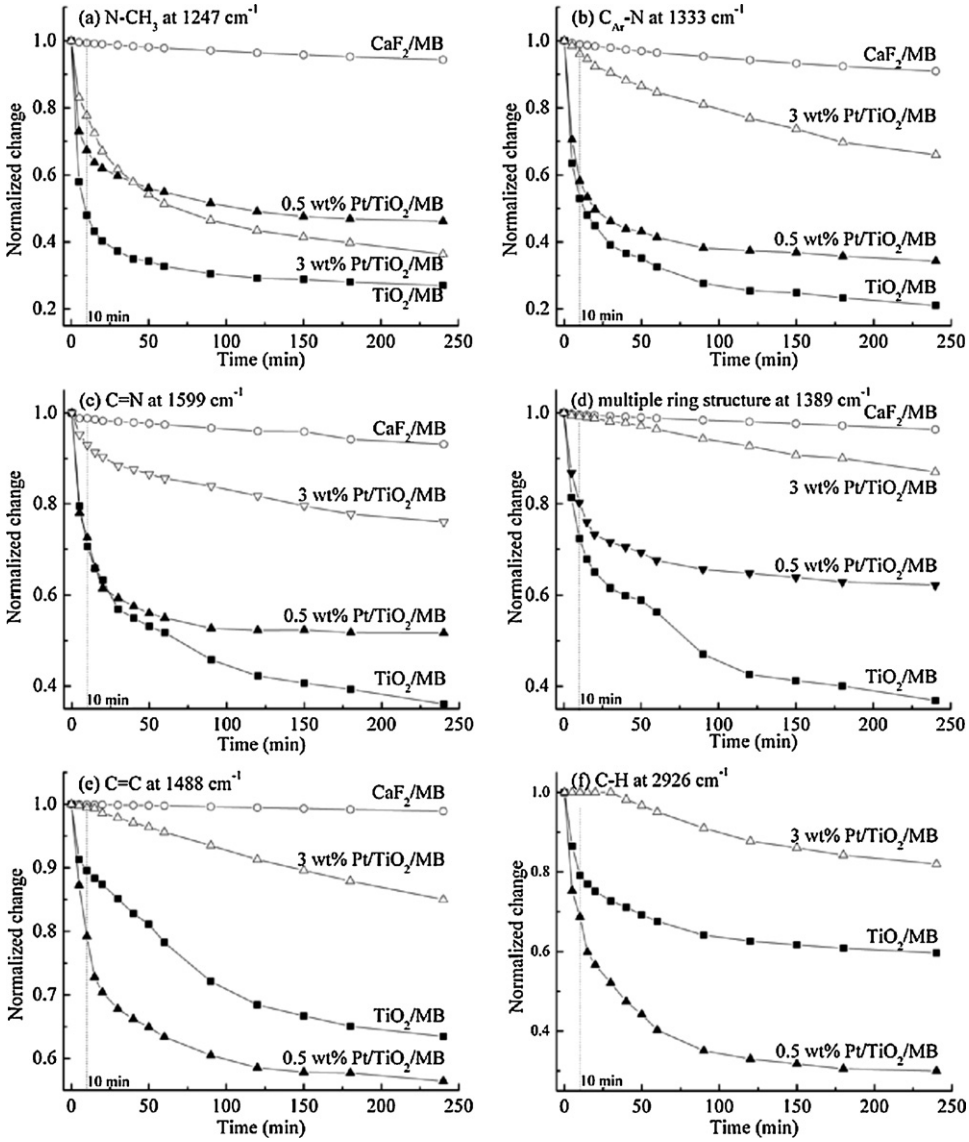

Fig. 9. Variations of the IR intensity of MB bands at (a) 1247, (b) 1333, (c) 1599, (d) 1389, (e) 1488, and (f) 2926 cm^{-1} during 240 min of the MB photocatalytic degradation.

4. Discussion

Fig. 12 presents the proposed reaction pathway for the $^{\bullet}OH$-initiating MB photocatalytic degradation. The pathway proposed here is consistent with that reported in our previous study [14]. $^{\bullet}OH$ has been shown to be produced from the reaction of H_2O_{ad} with photogenerated hole [42]. The major role of $^{\bullet}OH$ is to abstract H from organic compounds such as paraffins and aromatic hydrocarbons. Abstraction of hydrogen from $–CH_3$ by $^{\bullet}OH$ results in $–CH_3$ elimination and the concomitant N–H formation, as shown in step (i). $^{\bullet}OH$ could also attack N–H and C–H on the side benzene ring (step (ii)), facilitating the NH_4^+ formation and C_{Ar}–N scission. The MB central ring could further accept photogenerated electron and proton, as shown in step (iii), converting C=N and S=C to C–N and S–C, weakening the aromatic ring to facilitate its following breakup and reacting with $^{\bullet}OH$ and O_{ad} to produce CO_2, H_2O_{ad}, NH_4^+, and SO_4^{2-}.

Our previous studies have shown that the $^{\bullet}OH$-initiating photocatalytic degradation of organic compounds such as ethanol occurs on the H_2O-containing TiO_2 surface while h^+-initiating reactions take place on the H_2O-free TiO_2 surface [15]. H_2O adsorbs on the TiO_2 surface via heterolytic dissociation, resulting in hydrogen atom bonded to oxygen atom and –OH bonded to Ti atom (i.e., Ti–OH). Ti–OH on the TiO_2 surface could be in three different forms: linear around 3692 cm^{-1}, bridged around 3672 cm^{-1}, and triple-coordinated around 3632 cm^{-1} [43–45]. Ti–OH at 3632 cm^{-1} was displaced by adsorbed MB as shown by decrease in its intensity in Fig. 5 and Ti–OH at 3672 cm^{-1} was produced during the MB degradation, as shown by increase in its intensity in Figs. 6 and 7, suggesting that Ti–OH may be related to the photocatalytic degradation sites where $^{\bullet}OH$ is generated.

Although how –OH site is related to the site for $^{\bullet}OH$ generation remains unclear and $^{\bullet}OH$ can not be detected by IR, the rapid decay of C–H intensity in Fig. 9 accompanied by the

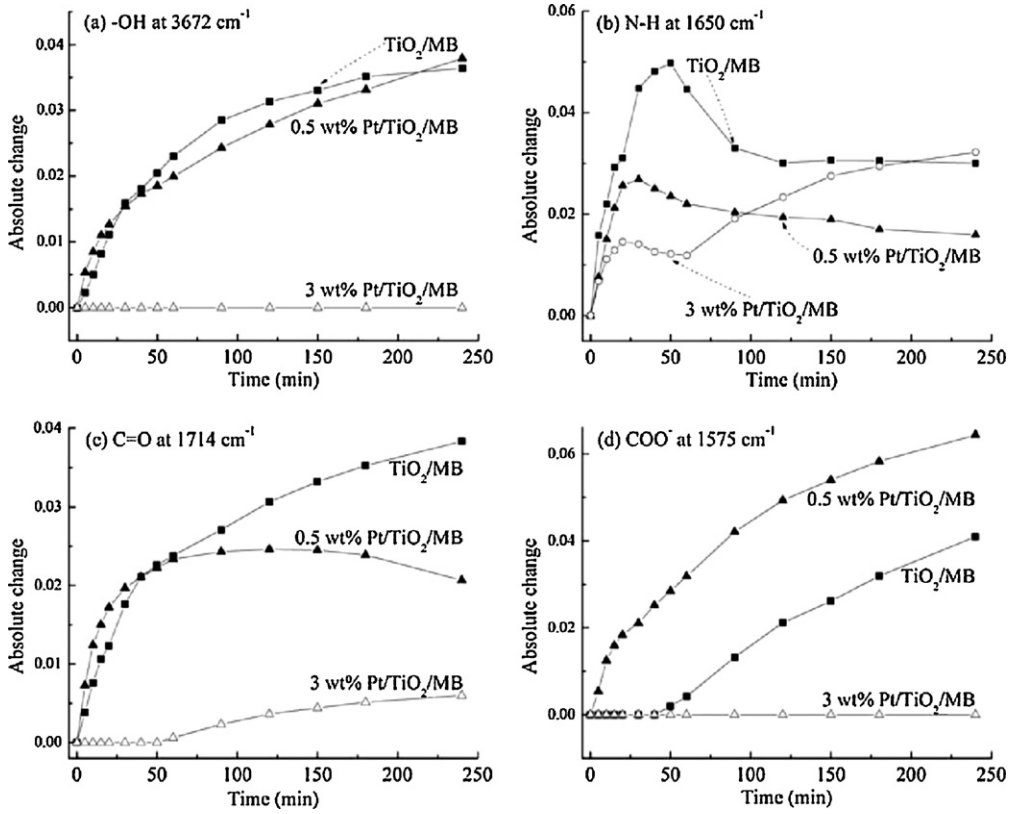

Fig. 10. Variations of the IR intensity of (a) –OH at 3672 cm^{-1}, (b) N–H at 1650 cm^{-1}, (c) C═O at 1714 cm^{-1}, and (d) COO^- at 1575 cm^{-1} during 240 min of the MB photocatalytic degradation.

rise of the Ti–OH intensity at 3672 cm^{-1} in Fig. 10 and H_2O_{ad} bands in Figs. 6 and 7 could be explained by the •OH-initiating photocatalytic degradation. In this pathway, •OH abstracts H from $–CH_3$, resulting in the formation of H_2O_{ad} which is further dissociated on the TiO_2 surface to generate Ti–OH at 3672 cm^{-1}. As the Ti sites are filled, physisorbed H_2O at 3550 cm^{-1} is formed on the top of Ti–OH. It has been shown

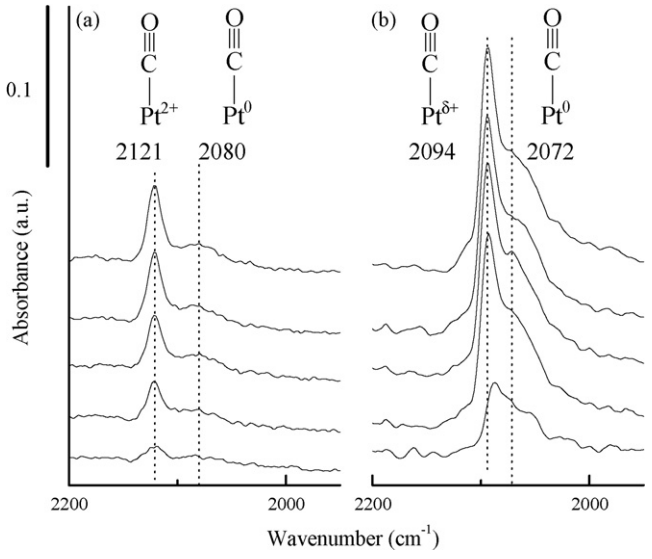

Fig. 11. IR spectra of CO adsorption over (a) 0.5 wt.% Pt/TiO_2 and (b) 3 wt.% Pt/TiO_2 as 1 mL CO pulse was admitted sequentially.

that H_2O dissociates on the TiO_2 (1 1 0) surface to generate Ti–OH and the second layer physisorbed H_2O blocks the interaction between O_2 and the TiO_2 surface [46]. The important role of –OH site in photocatalytic degradation is further substantiated by a negligible level of Ti–OH intensity at 3672 cm^{-1} on 3 wt.% Pt/TiO_2 which exhibited a zero initial activity for the abstraction of H from CH_3 on MB molecule.

The correlation between the increasing Ti–OH intensity and the decreasing C–H intensity provides not only an indirect evidence to support the •OH-initiating pathway but also an insight into the mechanism of the photoinduced hydrophilic conversion of the TiO_2 surface. The photoinduced hydrophilic conversion was first observed on the TiO_2 surface where the contact angle of water droplets on the TiO_2 surface changed from greater than 70° (i.e., hydrophobic) to less than 1° (i.e., hydrophilic) under UV illumination [47,48]. It is generally agreed that the removal of the hydrocarbon contaminants via photocatalytic oxidation is one of the main causes leading to the conversion of the hydrophobic to hydrophilic surface [49].

Due to the nature of hydrogen-bonding between the surface OH and H_2O molecule, it is reasonable to suggest that the increase in the hydrophilicity is a result of increase in the number of the surface OH group. XPS studies under high vacuum condition have shown that the amount of the surface OH increase with the hydrophilic conversion of the TiO_2 surface [50]. In contrast, IR studies show the absence of any change in the OH group on the TiO_2 surface during UV illumination, reaching the conclusion that photoinduced

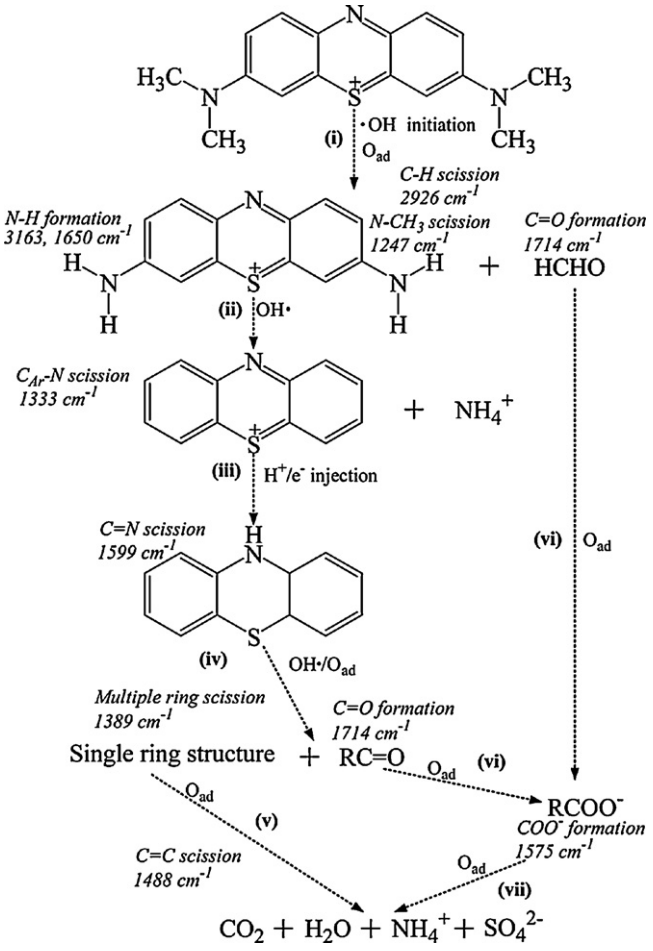

Fig. 12. Proposed pathway for the MB photocatalytic degradation.

hydrophilicity cannot be explained by the UV-induced change in the coverage and nature of the surface OH group [51]. Our observation of the formation of surface OH on the sites which was previously occupied by organics can lend itself to interpreting the source of incompatible conclusions drawing from results of studies involving different procedures and techniques to investigate photoinduced hydrophilicity [47–54].

Step (iii) in Fig. 12 suggests that the further breakup of MB central ring requires photogenerated electron and H^+ [14]. 3 wt.% Pt/TiO_2 showed a significantly low activity for breakup of the multiple ring structure, suggesting the lack of photogenerated electron and H^+ on 3 wt.% Pt/TiO_2 for weakening the MB central ring. Examining the TEM image of 3 wt.% Pt/TiO_2 in Fig. 3(b) shows a large portion of the TiO_2 surface on this catalyst was not covered by Pt, indicating that the Pt particles deposited by the photodeposition method were primarily located at the sites responsible for generation of $^{\bullet}OH$, H^+, and photogenerated electrons. The low activity of 3 wt.% Pt/TiO_2 for the MB degradation is consistent with the absence of Pt enhancement for photocatalytic oxidation of CO, suggesting high Pt loading resulted in the blocking of photocatalytic oxidation sites [55,56]. In addition to site blocking, excess Pt can absorb photons and act as a shield for the TiO_2 to adsorb UV illumination, resulting in screen-effect and decreasing the photoelectron generation [30,57]. The diminished reflectivity of Pt/TiO_2 as shown in Fig. 4 indicated the presence of screen-effect due to the Pt loading, which could also contribute to the lowered activity of 3 wt.% Pt/TiO_2 [58].

Pt exhibited its promoting function for scission of C=C and C–H bond as well as enhanced formation of COO^- on 0.5 wt.% Pt/TiO_2. IR single-beam spectra in Fig. 5 shows the presence of Ti–OH on 0.5 wt.% Pt/TiO_2; the difference spectra in Fig. 7 shows the formation of Ti–OH during the MB degradation, indicating the sites related to $^{\bullet}OH$ and photoelectron generation were not blocked by 0.5 wt.% Pt loading. The observed enhancement for bond scission and formation on 0.5 wt.% Pt/TiO_2 could be attributed to a synergetic role played by photoelectron generation, $^{\bullet}OH$ generation, and adsorbed oxygen on the Pt sites.

Due to the inability of infrared spectroscopy of the O_2^- species, its involvement in the oxidation has to be inferred from the dynamic behavior of the oxidation intermediates species which contain C=O and COO^-. Reduced Pt sites could dissociatively adsorb O_2 [5,59], catalyzing oxidation of C=C and C–H bonds in adsorbed species to reaction intermediates containing C=O and COO^- bonds [60]. Oxidized Pt sites which are associated with oxygen could undergo reduction to Pt° by accepting photogenerated electron and releasing oxygen for oxidation [19,61]. In addition, reduced Pt sites could facilitate the transfer of photogenerated electron, converting adsorbed oxygen to O_2^- [22]. The consumption of photogenerated electrons by adsorbed oxygen appears to precede the transfer of the electron to ring structure, resulting in a lower rate of ring breakup on 0.5 wt.% Pt/TiO_2 than TiO_2.

The different effects of Pt on the formation of the C=O and COO^- species, shown in Fig. 10, suggest that the nature of adsorbed oxygen involved in C=O formation is different from that in the formation of the COO^- species. Since the COO^- species contains negative charge, it is reasonable to postulate that the COO^- species is produced from O_2^-. The inability of the 3 wt.% Pt/TiO_2 to produce this COO^- species further substantiates that high Pt loading blocks the sites for generating photogenerated electrons for the step (2): $O_{2ad} + e^- \rightarrow O_2^-$.

5. Conclusions

The rates of decrease in IR intensities of specific bonds in MB molecule were compared and correlated with the rates of increase in IR intensities of reaction intermediates and –OH to unravel the Pt effect on MB photocatalytic degradation pathway on TiO_2. The rapid decay of C–H intensity accompanied by the rise of the Ti–OH intensity over TiO_2 and 0.5 wt.% Pt/TiO_2 provided an indirect evidence to support the $^{\bullet}OH$-initiating photocatalytic degradation pathway. The reaction of $^{\bullet}OH$ with MB molecule resulted in CH_3 elimination, N–H formation, and then C_{Ar}–N scission. The MB central ring could further accept protons and photogenerated electrons to facilitate its breakup and the resulting fragments reacted with $^{\bullet}OH$ and O_{ad} to produce CO_2, H_2O, NH_4^+, and SO_4^{2-}.

0.5 wt.% Pt/TiO_2 exhibited higher rates of C=C and C–H scission as well as COO^- formation than TiO_2 whereas 3 wt.% Pt/TiO_2 showed a significantly low activity for all the MB bond

scission. The low activity of 3 wt.% Pt/TiO_2 was directly correlated with a negligible level of –OH at 3632 cm^{-1} before the reaction and the absence of –OH at 3672 cm^{-1} during the reaction, suggesting the –OH absorption sites could be related to $^{\bullet}OH$ generation sites. The sites related to these two types of –OH are needed for high rate of photocatalytic degradation. The high activity of 0.5 wt.% Pt/TiO_2 can be attributed to the presence of $^{\bullet}OH$ generation sites and Pt sites, where Pt provided O_{ad} for oxidizing the fragments from breakup of MB molecule to intermediates containing C=O and COO^- groups. The effective use of Pt for promoting photocatalytic degradation requires minimizing the blocking of active sites by Pt deposition.

Acknowledgments

This work was partially supported by the Ohio Board of Regents (Grant R4552-OBR) and the US Department of Energy (Grant DE-FG26-01NT41294).

References

[1] P.V. Kamat, Chem. Rev. 93 (1993) 267–300.
[2] M.A. Fox, M.T. Dulay, Chem. Rev. 93 (1993) 341–357.
[3] M.R. Hoffmann, S.T. Martin, W. Choi, D.W. Bahnemann, Chem. Rev. 95 (1995) 69–96.
[4] A.L. Linsebigler, G. Lu, J.T. Yates Jr., Chem. Rev. 95 (1995) 735–758.
[5] B. Sun, A.V. Vorontsov, P.G. Smirniotis, Langmuir 19 (2003) 3151–3156.
[6] Y. Chen, D.D. Dionysiou, Appl. Catal. B 62 (2006) 255–264.
[7] R. Nakamura, Y. Nakato, JACS 126 (2004) 1290–1298.
[8] R. Nakamura, T. Okamura, N. Ohashi, A. Imanishi, Y. Nakato, JACS 127 (2005) 12975–12983.
[9] K. Ikeda, H. Sakai, R. Baba, K. Hashimoto, A. Fujishima, J. Phys. Chem. B 101 (1997) 2617–2620.
[10] D.-R. Park, J. Zhang, K. Ikeue, H. Yamashita, M. Anpo, J. Catal. 185 (1999) 114–119.
[11] O.M. Alfano, M.I. Cabrera, A.E. Cassano, J. Catal. 172 (1997) 370–379.
[12] M.C. Lee, W. Choi, J. Phys. Chem. B 106 (2002) 11818–11822.
[13] M.M. Ameen, G.B. Raupp, J. Catal. 184 (1999) 112–122.
[14] Z. Yu, S.S.C. Chuang, J. Phys. Chem. C 111 (2007) 13813–13820.
[15] Z. Yu, S.S.C. Chuang, J. Catal. 246 (2007) 118–126.
[16] G. Balasubramanian, D.D. Dionysiou, M.T. Suidan, I. Baudin, J.-M. Laine, Appl. Catal. B 47 (2004) 73–84.
[17] S.H. Szczepankiewicz, J.A. Moss, M.R. Hoffmann, J. Phys. Chem. B 106 (2002) 2922–2927.
[18] W. Zhao, W. Ma, C. Chen, J. Zhao, Z. Shuai, JACS 126 (2004) 4782–4783.
[19] J. Lee, W. Choi, J. Phys. Chem. B 109 (2005) 7399–7406.
[20] R. Asahi, T. Morikawa, T. Ohwaki, K. Aoki, Y. Taga, Science 293 (2001) 269–271.
[21] H. Park, J. Lee, W. Choi, Catal. Today 111 (2006) 259–265.
[22] W. Zhao, C. Chen, X. Li, J. Zhao, H. Hidaka, N. Serpone, J. Phys. Chem. B 106 (2002) 5022–5028.
[23] S. Hwang, M.C. Lee, W. Choi, Appl. Catal. B 46 (2003) 49–63.
[24] S. Kim, W. Choi, J. Phys. Chem. B 106 (2002) 13311–13317.
[25] H. Haick, Y. Paz, J. Phys. Chem. B 107 (2003) 2319–2326.
[26] V. Keller, P. Bernhardt, F. Garin, J. Catal. 215 (2003) 129–138.
[27] S. Sakthivel, M.V. Shankar, M. Palanichamy, B. Arabindoo, D.W. Bahnemann, V. Murugesan, Water Res. 38 (2004) 3001–3008.
[28] A.V. Vorontsov, I.V. Stoyanova, D.V. Kozlov, V.I. Simagina, E.N. Savinov, J. Catal. 189 (2000) 360–369.
[29] F. Denny, J. Scott, K. Chiang, W.Y. Teoh, R. Amal, J. Mol. Catal. A: Chem. 263 (2007) 93–102.
[30] C.A. Emilio, M.I. Litter, M. Kunst, M. Bouchard, C. Colbeau-Justin, Langmuir 22 (2006) 3606–3613.
[31] F.B. Li, X.Z. Li, Chemosphere 48 (2002) 1103–1111.
[32] H. Park, W. Choi, J. Phys. Chem. B 109 (2005) 11667–11674.
[33] H. Lachheb, E. Puzenat, A. Houas, M. Ksibi, E. Elaloui, C. Guillard, J.-M. Herrmann, Appl. Catal. B 39 (2002) 75–90.
[34] T. Zhang, T. Oyama, A. Aoshima, H. Hidaka, J. Zhao, N. Serpone, J. Photochem. Photobiol. A 140 (2001) 163–172.
[35] J.L. Falconer, K.A. Magrini-Bair, J. Catal. 179 (1998) 171–178.
[36] J.C. Kennedy III, A.K. Datye, J. Catal. 179 (1998) 375–389.
[37] R.W. Stevens, S.S.C. Chuang, B.H. Davis, Thermochim. Acta 407 (2003) 61–71.
[38] K. Tanaka, J.M. White, J. Catal. 79 (1983) 81–94.
[39] P. Panagiotopoulou, A. Christodoulakis, D.I. Kondarides, S. Boghosian, J. Catal. 240 (2006) 114–125.
[40] K. Almusaiteer, S.S.C. Chuang, J. Catal. 184 (1999) 189–201.
[41] C. Hu, Y. Tang, J. Zheng, Z. Hao, H. Tang, P.K. Wong, Appl. Catal. A 253 (2003) 389–396.
[42] Y. Murakami, E. Kenji, A.Y. Nosaka, Y. Nosaka, J. Phys. Chem. B 110 (2006) 16808–16811.
[43] K.I. Hadjiivanov, D.G. Klissurski, Chem. Soc. Rev. 25 (1996) 61–69.
[44] A. Davydov, Molecular Spectroscopy of Oxide Catalyst Surfaces, Wiley, Hoboken, 2003.
[45] N.B. Colthup, L.H. Daly, S.E. Wiberley, Introduction to Infrared and Raman Spectroscopy, 3rd ed., Academic Press, Boston, 1990.
[46] M.A. Henderson, W.S. Epling, C.H.F. Peden, C.L. Perkins, J. Phys. Chem. B 107 (2003) 534–545.
[47] R. Wang, K. Hashimoto, A. Fujishima, M. Chikuni, E. Kojima, A. Kitamura, M. Shimohigoshi, T. Watanabe, Adv. Mater. 10 (1998) 135.
[48] R. Wang, K. Hashimoto, A. Fujishima, M. Chikuni, E. Kojima, A. Kitamura, M. Shimohigoshi, T. Watanabe, Nature (1997) 431–432.
[49] T.L. Thompson, J.T. Yates Jr., Chem. Rev. 106 (2006) 4428–4453.
[50] N. Sakai, A. Fujishima, T. Watanabe, K. Hashimoto, J. Phys. Chem. B 107 (2003) 1028–1035.
[51] T. Zubkov, D. Stahl, T.L. Thompson, D. Panayotov, O. Diwald, J.T. Yates Jr., J. Phys. Chem. B 109 (2005) 15454–15462.
[52] R.D. Sun, A. Nakajima, A. Fujishima, T. Watanabe, K. Hashimoto, J. Phys. Chem. B 105 (2001) 1984–1990.
[53] M. Miyauchi, A. Nakajima, A. Fujishima, K. Hashimoto, T. Watanabe, Chem. Mater. 12 (2000) 3–5.
[54] Y.F. Gao, Y. Masuda, K. Koumoto, Langmuir 20 (2004) 3188–3194.
[55] A. Linsebigler, C. Rusu, J.T. Yates Jr., JACS 118 (1996) 5284–5289.
[56] C. Chan Sze, A. Barteau Mark, Langmuir 21 (2005) 5588–5595.
[57] A. Maldotti, A. Molinari, G. Varani, M. Lenarda, L. Storaro, F. Bigi, R. Maggi, A. Mazzacani, G. Sartori, J. Catal. 209 (2002) 210–216.
[58] I. Bouzaida, C. Ferronato, J.M. Chovelon, M.E. Rammah, J.M. Herrmann, J. Photochem. Photobiol. A 168 (2004) 23–30.
[59] S.S.C. Chuang, C.-D. Tan, J. Phys. Chem. B 101 (1997) 3000–3004.
[60] M.C. Blount, J.L. Falconer, J. Catal. 200 (2001) 21–33.
[61] V. Subramanian, E.E. Wolf, P.V. Kamat, Langmuir 19 (2003) 469–474.
[62] T.C.K. Yang, S.F. Wang, S.H.Y. Tsai, S.Y. Lin, Appl. Catal. B 30 (2001) 293–301.
[63] J.M. Gallardo Amores, V. Sanchez Escribano, G. Ramis, G. Busca, Appl. Catal. B 13 (1997) 45–58.
[64] J.M. Coronado, S. Kataoka, I. Tejedor-Tejedor, M.A. Anderson, J. Catal. 219 (2003) 219–230.
[65] A.C. Lukaski, D.S. Muggli, J. Catal. 223 (2004) 250–261.